Reduced early Holocene moisture availability inferred from D values of sedimentary n-alkanes in Zigetang Co, Central...

6 authors, including:

Chuanfang Jin
Chinese Academy of Sciences
4 PUBLICATIONS   5 CITATIONS

SEE PROFILE

Shijie Li
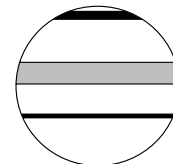Chinese Academy of Sciences
47 PUBLICATIONS   696 CITATIONS

SEE PROFILE

Guodong Jia
Tongji University
100 PUBLICATIONS   1,331 CITATIONS

SEE PROFILE

Reduced early Holocene moisture availability inferred from δD values of sedimentary *n*-alkanes in Zigetang Co, Central Tibetan Plateau

Chuanfang Jin,[1,2] Franziska Günther,[3] Shijie Li,[1,4] Guodong Jia,[5] Ping'an Peng[5] and Gerd Gleixner[3]

Abstract

An 885-cm-long laminated sediment core was retrieved from Zigetang Co, a non-glacial meltwater-fed lake in the central Tibetan Plateau, and analyzed for *n*-alkanes as well as their hydrogen isotopes to trace the regional climatic and environmental history spanning the last 13.8 cal. ka BP. The short-chain *n*-alkanes $C_{15/16/17}$, likely derived from aquatic algae, plankton, and photosynthetic bacteria, dominate the *n*-alkane composition in this lake. This unusual distribution pattern might be attributed to the meromictic lake system that is characterized by a rapid salinity increase and an abrupt decrease in dissolved oxygen in the lake water with depth, as well as anoxic conditions at the bottom. *n*-Alkane indicator ratios (e.g. carbon preference index (CPI), average chain length (ACL), and aquatic/terrigenous ratio (ATR)) and δD values reveal that higher effective moisture availability at Zigetang Co occurred in the middle (5.8–2.7 cal. ka BP) rather than the early Holocene. This contradicts palaeoclimate records from neighboring lakes (e.g. Nam Co, Siling Co, and Paru Co). We suggest that in the Zigetang Co catchment where glacial meltwaters are not available, the temperature-induced evaporation would outweigh the monsoonal precipitation and, therefore, result in lower effective moisture displayed by the increasing δD values during the early Holocene. The local recycling of air masses could also have an important impact on the lake level and moisture availability and cannot be excluded. Our record provides further evidence for the complex relationship of insolation-induced temperature, evaporation, and precipitation affecting the regional climate changes on the Tibetan Plateau.

Introduction

n-Alkanes, stable lipid molecular fossils, are derived from various organisms such as bacteria and algae living in the water column (Han and Calvin, 1969; Meyers, 2003), aquatic macrophytes (Cranwell et al., 1987; Ficken et al., 2000), or terrestrial vascular plants (Eglinton and Hamilton, 1967; Rieley et al., 1991). Compound-specific hydrogen isotopes of sedimentary *n*-alkanes reflect isotopic values from water sources and atmospheric precipitation, which are strongly influenced by temperature, rainfall, moisture, biology, and other factors (Huang et al., 2004; Sachse et al., 2012; Schefuss et al., 2005). With the advancements in the field of gas chromatography (GC)/thermal conversion (TC)/isotope ratio mass spectrometry (IRMS), *n*-alkanes and their individual hydrogen isotopes provide geochemical proxies for palaeoclimatic and palaeoenvironmental reconstruction. They have been widely used for corals (Bouloubassi et al., 1992), stalagmites (Blyth et al., 2011), loess (Liu and Huang, 2005; Xie et al., 2003), peat deposits (Seki et al., 2009; Zheng et al., 2007), ice cores (Thompson et al., 2000; Xie et al., 2000), lake sediments (Günther et al., 2015; Mügler et al., 2010), marine sediments (Jeng, 2006; Peleiero, 2003), and other geological archives in recent years.

The Tibetan Plateau plays an important role in the climate and environmental evolution of East-South Asia, in the formation and development of the Asian Monsoon, and in the evolution of circulation in the Northern Hemisphere (Kutzbach et al., 1993; Liu et al., 2003). The numerous lakes on the Tibetan Plateau provide

[1]State Key Laboratory of Lake Science and Environment, Nanjing Institute of Geography and Limnology, Chinese Academy of Sciences, China
[2]University of Chinese Academy of Sciences, China
[3]Max Planck Institute for Biogeochemistry, Germany
[4]State Key Laboratory of Environmental Geochemistry, Institute of Geochemistry, Chinese Academy of Sciences, China
[5]Guangzhou Institute of Geochemistry, Chinese Academy of Sciences, China

Corresponding authors:
Shijie Li, State Key Laboratory of Environment Geochemistry, Institute of Geochemistry, Chinese Academy of Sciences, Guiyang 550002, China.
Emails: lishijie@vip.gyig.ac.cn

Gerd Gleixner, Max Planck Institute for Biogeochemistry, Jena 07745, Germany.
Email: gerd.gleixner@bgc-jena.mpg.de
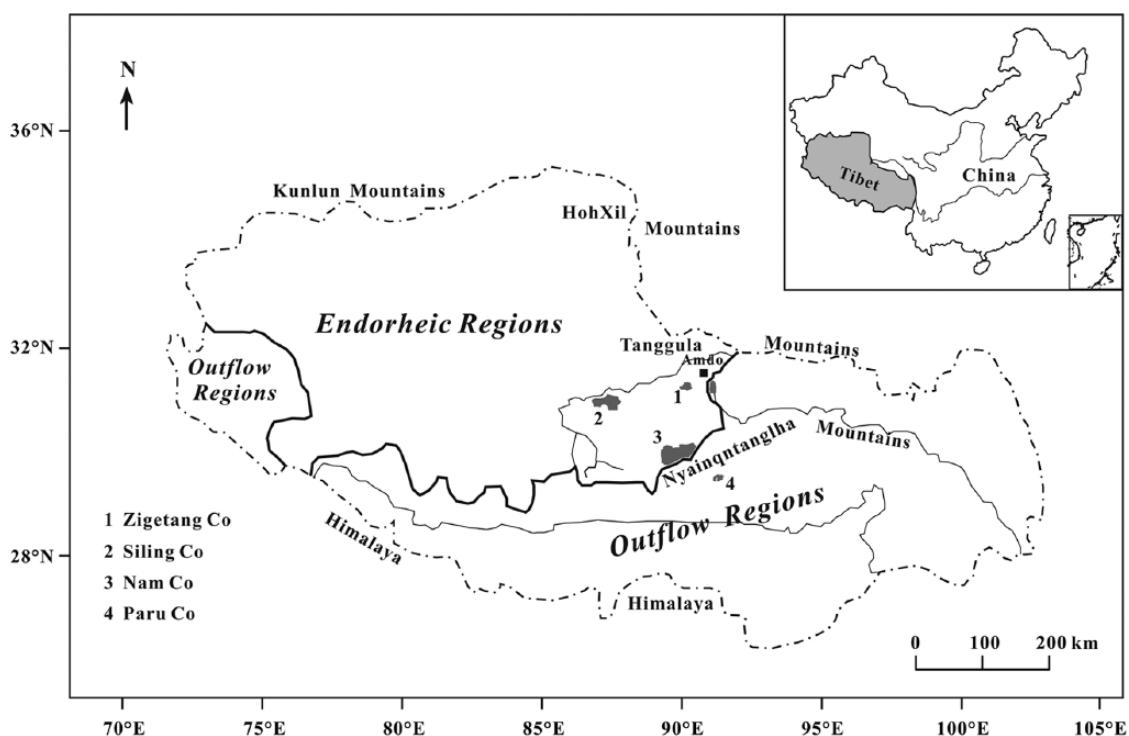
Figure 1. Map showing the location of Zigetang Co and other nearby lakes mentioned in the text such as Paru Co (Bird et al., 2014), Nam Co (Günther et al., 2015; Mügler et al., 2010), and Siling Co (Gu et al., 1993).

excellent and high-resolution archives for climate and environment variations over various geological periods because of their high sensitivity to climate changes and the low impact of human activities (Miehe et al., 2006; Yao and Zhu, 2006). In the last decade, sedimentary *n*-alkanes and their individual hydrogen isotopes were increasingly applied to reconstruct the palaeoclimate and palaeoenvironment in the Tibetan lake systems (e.g. Aichner et al., 2010; Bird et al., 2014; Günther et al., 2011; Wang et al., 2013; Zhu et al., 2008).

Several projects have revealed that the strongest summer monsoon occurred in combination with warm and humid conditions during the early Holocene on the Tibetan Plateau (e.g. Shen et al., 2005; Zhou et al., 2004). However, the exact timing, duration, and amplitudes of the Holocene monsoon maximum appear to vary in different regions. Pollen records from the Zoige Basin, for example, show that the maximum monsoon occurred in the middle rather than the early Holocene (Zhao et al., 2011). Further analysis based on Chinese cave records indicates the maximum precipitation intensity seems to take place much later after the summer insolation maximum in the region between Dongge and Heshang caves (Hu et al., 2008). Possible reasons for such spatial heterogeneities are not well known and need to be investigated through additional regional records. In our study, we present a terminal Pleistocene and Holocene record of lacustrine sediments from Zigetang Co, a meromictic endorheic saline lake in the central Tibetan Plateau. The lake is not influenced by glacial meltwater and, hence, only reflects changes in the precipitation–evaporation signal. Many studies have been done on this lake in recent years including pollen (Herzschuh et al., 2006), geochemistry (Wu et al., 2007), carbonate and soluble salt (Li et al., 2009), and ostracod shell stable isotope (Zhang et al., 2014). For the first time, sedimentary *n*-alkanes and compound-specific stable hydrogen isotopes are analyzed to investigate the local climate and moisture evolution as well as their potential driving factors in the region without any buffering capacity of glaciers. Our record provides additional information with respect to the unusual distribution pattern of sedimentary *n*-alkanes in the lake and improves the

understanding of complicated climatological changes on the Tibetan Plateau.

Study area

The meromictic Lake Zigetang Co (32°00′~32°09′N, 90°44′~90°57′E, 4561 m a.s.l.) is situated in the central Tibetan Plateau, southern Tanggula Mountains, and belongs to Amdo County, Xizang Autonomous Region, China (Figure 1). It was formed along Bangong Lake–Dongqiao–Nujiang River fault zone in the late Pliocene (Guan et al., 1984). The lake is 9.5 km long from north to south and 20.2 km wide from east to west, with a surface area of 191.4 km². The hydrological system drains a total watershed of 3430 km² with a landscape of hills, plains, and desert grasslands (Wang and Dou, 1998). The average water depth is 19.2 m with a maximum of 38.9 m (measured in August of 2012). As a result of the missing glacial meltwater inputs, the water supply only depends on precipitation and seasonal inflows. Chairongzangbu is the longest stream into the lake draining with more than 42% of the catchment area (Figure 2a).

The present climate in the catchment of Zigetang Co is cold and semi-arid. Meteorological data from Amdo station (4800 m a.s.l., ~100 km east of the lake) and Bange station (4701 m a.s.l., ~100 km southwest of the lake) indicate a mean annual temperature of approximately −3.3 to 0.1°C (mean July temperature: 7.9–9.3°C; mean January temperature: −14.2 to −12.2°C) in the basin and mean annual precipitation of 240–500 mm that mainly falls in summer (Figure 3). The average annual evaporation ranges between 791 and 1112 mm (Li et al., 2001a). Alpine steppe soils and desert soils dominate the lake catchment. The vegetation surrounding the lake is typical for arid, high-altitude climate and primarily consists of alpine grasslands and meadows such as *Stipa L., Carex L.*, and *Artemisia L.* (Herzschuh et al., 2006). The lake is stratified with an anoxic bottom layer below 15 m water depth (measured with Yellow Spring Instrument 6600 V2 multisensor sonde in 2012) with pH values between 9.9 and 10.2. The average salinity of the lake water is 41.1 g/L, representing a typical saline lake dominated by Na^+ and HCO_3^- ions (Li and Li,
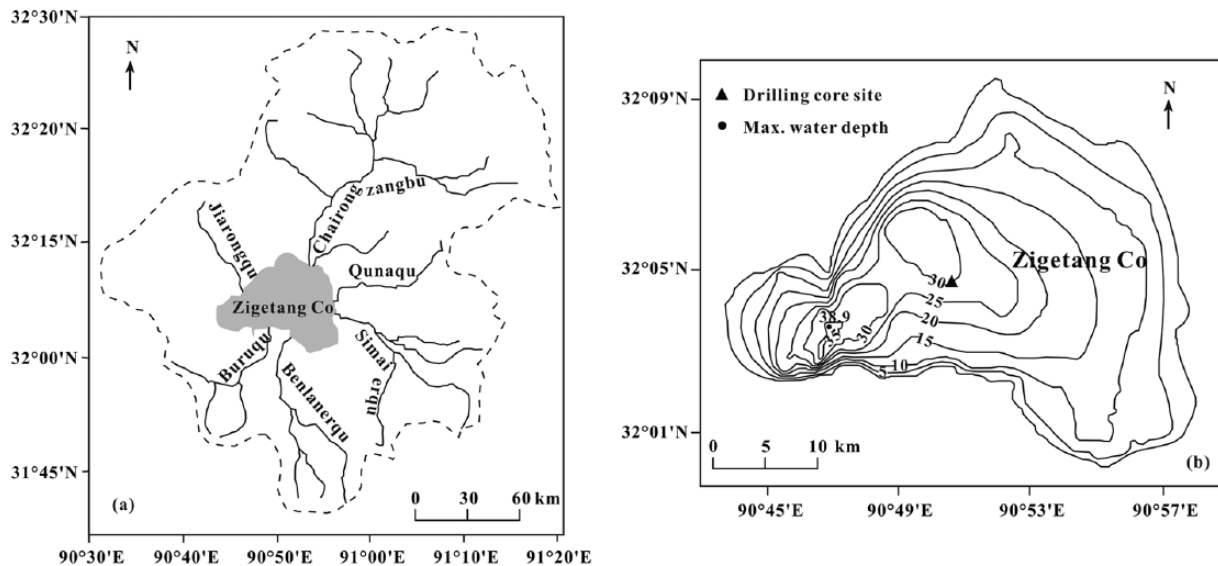
Figure 2. Overview map of (a) the Zigetang Co catchment and (b) drilling core site within the lake in August 2012.
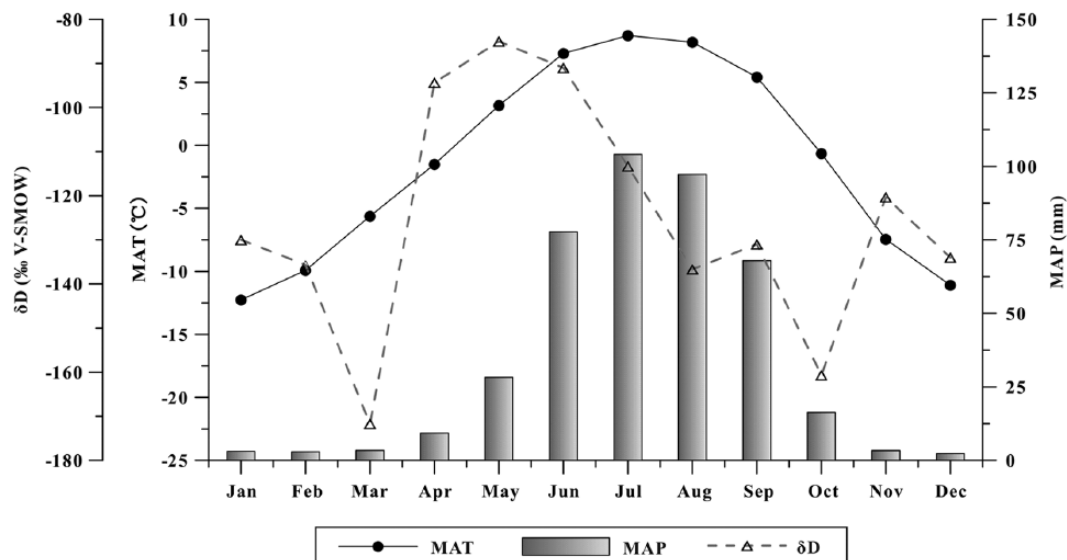

Figure 3. Average monthly temperatures (solid line) and precipitation amounts (blank boxes) at meteorological stations (Amdo and Bange stations) from 1978 to 2008. The dashed line indicates seasonal variation in hydrogen isotope (δD) of precipitation at 32°N, 90°E, and 4561 m a.s.l., calculated using the Online Isotopes in Precipitation Calculator (OIPC). MAT represents mean annual temperature and MAP represents mean annual precipitation.

2004). A summary of meteorological and limnological data of Zigetang Co is given in Table 1.

Materials and methodology

Sample collection and preparation

In August 2012, the 885-cm-long sediment core ZGT12/02 (32.0°N, 90.9°E) was taken from the western central basin of the lake at about 29 m water depth using a piston corer (Figure 2b). The drilled core was split, photographed, described, and sampled at 1 cm intervals (corresponding to a resolution of around 12.5 years) in the State Key Laboratory of Environment, Geochemistry Institute, Chinese Academy of Sciences, China. The fresh core colors mainly include gray, dark-gray, and black layers. Oxidized sediments display a clear stratification, which indicates stable and continuous sedimentary evolution. The sediments are rich in carbonate mud with distinct regular laminations throughout the profile. The collected samples were freeze-dried, ground to grain size <100 μm, and kept frozen for further analysis.

Sediment chronology

A total of 13 bulk sediment samples were collected for ^{14}C-accelerator mass spectrometry (AMS) dating in the Beta Analytic Laboratory, Miami, USA. AMS ^{14}C data were significantly linearly correlated with depths of samples, displaying slight variations of sedimentation rate covering the investigated time scales (Table 2). In Tibetan lake systems, the reliable age model is frequently hampered by the existence of reservoir effects (Hou et al., 2012). Based on surface sediment ages, a constant reservoir correction of 2060 ± 50 years was applied to the radiocarbon ages in Zigetang Co before they were calibrated (Wu et al., 2007). For this study, the radiocarbon ages were calibrated and the age–depth model was established using classical age–depth modeling (CLAM) in R software (Figure 4). One outlier was recognized following the guidance of Bpeat software (Blaauw, 2010; Blaauw and Christen, 2005). The smooth-spline method in CLAM was adopted for the age model with a smoothing level of 0.3. A best fit age (solid line in Figure 4) and uncertainty ranges (95% confidence intervals, dashed lines in Figure 4) were produced by this model. Confidence

intervals were calculated at 2 standard deviation (95%) level based on 10,000 iterations. The model indicates that the sedimentary record reaches back to approximately 13.8 cal. ka BP with an average sedimentation rate of 0.8 mm/yr.

Analytical methods

n-Alkane analysis. Sample treatment and analysis were carried out at the Max Planck Institute for Biogeochemistry, Jena, Germany. About 2 g of dry sediments was used for total lipid extraction with accelerated solvent extractor (ASE-200; DIONEX Corp., Sunnyvale, USA). The ASE was operated with dichloromethane/methanol (9:1, v/v) at 100°C and 2000 psi (138 bar) for 15 min in two cycles. The total lipid extract was separated into four fractions (aliphatics, aromatics, alcohols, and other compounds) using activated silica gel column chromatography (0.040–0.063 mm mesh) and eluted with hexane, hexane/dichloromethane (1:1, v/v), dichloromethane/methanol (1:1, v/v), and methanol, respectively. Additionally, the elemental sulfur was removed by the addition of activated copper (Cu 99%; Acros Organics, Belgium, USA).

n-Alkanes were identified and quantified by GC with flame ionization detection (TRACE-GC 2000; CE Instruments, Thermo

Table 1. General geographical, climatological, and limnological properties of Zigetang Co.

Latitude	32°00′–32°09′N
Longitude	99°44′–90°57′E
Altitude	4561 m a.s.l.
Lake surface area	191.4 km^2
Catchment area	3430 km^2
Max. depth[a]	38.9 m
Depth at core site[a]	30 m
Mean annual temperature[b]	−3.3 to 0.1°C (AD 1978–2008)
Mean annual precipitation[b]	240–500 mm (AD 1978–2008)
Mean annual evaporation[c]	791–1112 mm
Water temperature[a]	2.3–15.4°C
Dissolved oxygen[a]	1.1–7.8 mg/L
Electrical conductivity[a]	0.1–24.3 mS/cm
pH[a]	9.9–10.2
Salinity[d]	41.1 g/L

[a]Measured in August of 2012.
[b]Meteorological records from Amdo and Bange stations.
[c]Li et al. (2001a).
[d]Li and Li (2004).

Quest, Rodano, Italy), based on retention times and comparison with an external *n*-alkane standard mixture (*n*-C$_{15}$ to *n*-C$_{33}$). The gas chromatograph was equipped with a DB1ms column (30 m, ID: 0.25 mm, film thickness: 0.25 μm; Agilent Technologies, Santa Clara, USA). Helium was used as carrier gas at constant flow of 1.3 mL/min. The PTV injector was operated in constant temperature mode at 280°C with a split ratio of 1:10. The GC oven was maintained for 1 min at 140°C, then raised to 300°C at a rate of 10°C/min (held for 9 min), and finally heated up to 335°C at a rate of 30°C/min (held for 3 min).

Principal component analysis (PCA) was applied to analyze variations in the *n*-alkane distribution using Canoco 4.5 software. In addition, *n*-alkane indicator ratios were calculated using the amount of the respective compounds according to the following equations.

Carbon preference index (CPI) (Bray and Evans, 1961):

$$CPI_{16-32} = \frac{1}{2} \times \left[\frac{\left(\sum_{odd} C_{17-31}\right)}{\left(\sum_{even} C_{16-30}\right)} + \frac{\left(\sum_{odd} C_{17-31}\right)}{\left(\sum_{even} C_{18-32}\right)} \right] \quad (1)$$

Average chain length (ACL) (Poynter and Eglinton, 1990):

$$ACL_{15-33} = \frac{\sum\left(C_n \times n\right)}{\sum C_n} \quad (2)$$

Aquatic/terrigenous ratio (ATR) (Meyers, 1997):

$$ATR = \frac{\left(n-C_{15} + n-C_{17} + n-C_{19}\right)}{\left(n-C_{27} + n-C_{29} + n-C_{31}\right)} \quad (3)$$

δD$_{n-alkanes}$ measurement. Hydrogen isotope ratios of individual *n*-alkanes were determined using a coupled GC-IRMS system (GC: HP7890, Agilent Technologies, Palo Alto, USA; IRMS: Delta V Plus Isotope Ratio MS, Thermo Fisher Scientific, Bremen, Germany). The GC was equipped with a DB1ms column (30 m, ID: 0.25 mm, film thickness: 0.25 μm; Agilent Technologies) and helium as carrier gas. The injector was operated at 280°C in a splitless mode. The oven temperature was programmed to be held initially at 110°C for 1 min, then heated with 5°C/min to 320°C (held for 8 min), and finally heated with 30°C/min to 335°C (held for 2 min). The column flow was constant at 1.3 mL/min throughout the run. The δD values were determined at least three times for each sample and normalized to the Vienna Standard Mean Ocean Water (V-SMOW) scale using a mixture of *n*-alkanes (*n*-C$_{15}$ to *n*-C$_{33}$). To ensure the accuracy of the analysis, the

Table 2. Accelerator mass spectrometry radiometric data for Zigetang Co.

Sample number	Depth (cm)	Material	^{14}C age (yr BP)	Reservoir-corrected ^{14}C age (yr BP)	Calendar age (cal. yr BP)
ZGT2-70	69.5	OM$_{bulk}$	3080 ± 30	1020 ± 30	941 ± 30
ZGT2-141	140.5	OM$_{bulk}$	3830 ± 30	1770 ± 30	1675 ± 30
ZGT2-209	208.5	OM$_{bulk}$	4880 ± 30	2820 ± 30	2921 ± 30
ZGT2-281	280.5	OM$_{bulk}$	5740 ± 30	3680 ± 30	4024 ± 30
ZGT2-350	349.5	OM$_{bulk}$	6840 ± 30	4780 ± 30	5518 ± 30
ZGT2-422	421.5	OM$_{bulk}$	7320 ± 30	5260 ± 30	6022 ± 30
ZGT2-491	490.5	OM$_{bulk}$	8270 ± 40	6210 ± 40	7102 ± 40
ZGT2-572	571.5	OM$_{bulk}$	10,230 ± 30	8170 ± 30	9099 ± 30
ZGT2-610	609.5	OM$_{bulk}$	11,340 ± 50	9280 ± 50	10,463 ± 50
ZGT2-680[a]	679.5	OM$_{bulk}$	12,790 ± 50	10,730 ± 50	12,679 ± 50
ZGT2-754	753.5	OM$_{bulk}$	12,490 ± 50	10,430 ± 50	12,311 ± 50
ZGT2-812	811.5	OM$_{bulk}$	13,120 ± 50	11,060 ± 50	12,925 ± 50
ZGT2-885	884.5	OM$_{bulk}$	14,100 ± 50	12,040 ± 50	13,888 ± 50

[a]Excluded from the age model.
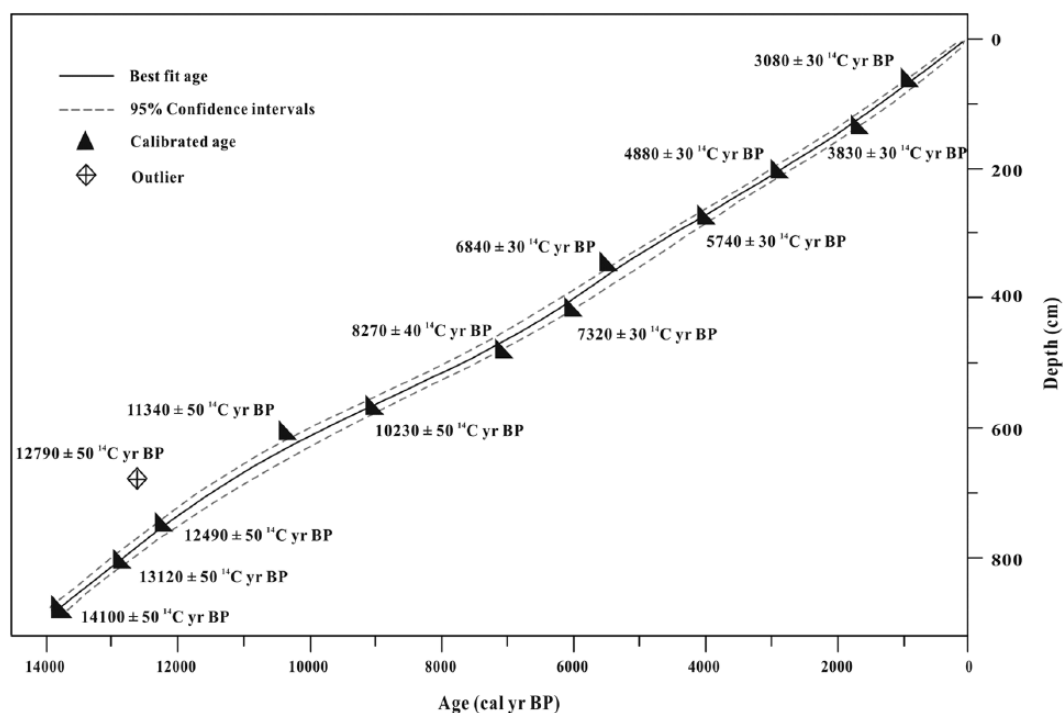
Figure 4. Age–depth model for sediment core from Zigetang Co (in calibrated years BP) using a smooth-spline model in CLAM (smoothing factor, 0.3). Dashed lines show 95% confidence intervals. Solid line shows the 'best' fit of the age estimates. A modern age was assumed for the sediment surface and a constant 2060±50 years reservoir effect was used in the age model (Wu et al., 2007).
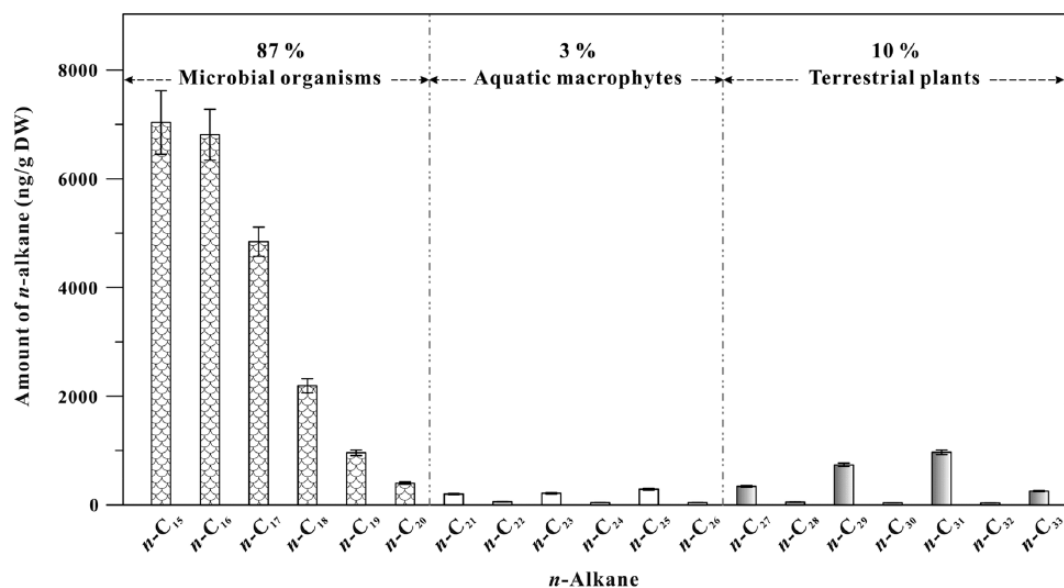
Figure 5. Mean concentration and composition of *n*-alkanes in the lake sediments from Zigetang Co. Error bars indicate standard errors.

standard mixture was measured independently three times after the measurement of three samples at the most. The H_3^+ factor was determined once a day and stayed constant at 3.2 with a standard deviation of 0.5 during the measurement period.
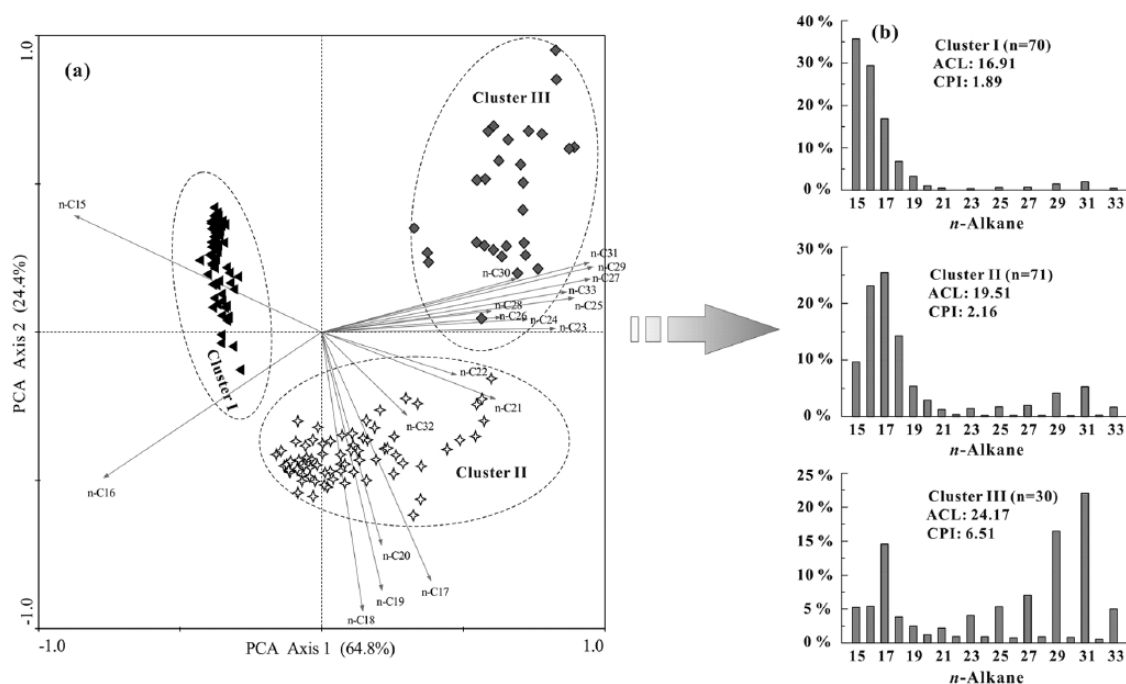
# Results

n-Alkane distribution of lacustrine sediments

The *n*-alkanes in the lake sediments range from *n*-C_{15} to *n*-C_{33} with a clear predominance of the short-chain *n*-alkanes $C_{15/16/17}$ (Figure 5). The lower carbon–numbered *n*-alkanes exhibit no apparent odd over even carbon predominance, resulting in lower $CPI_{15–20}$ values of 0.91–3.94, whereas the higher carbon–numbered *n*-alkanes have distinct odd carbon preference with higher

$CPI_{21–32}$ values of 4.85–19.78. The mean concentration of alkanes *n*-$C_{15–33}$ varies between 38 and 7038 ng/g dry weight. On average, the short-chain alkanes *n*-$C_{15–20}$ account for 87%, the middle-chain alkanes *n*-$C_{21–26}$ for 3%, and the long-chain alkanes *n*-$C_{27–33}$ for 10%. Because of the predominance of short-chain *n*-alkanes over the sediment core, changes in the amount of *n*-alkanes $C_{15–33}$ resemble variations in the amount of *n*-alkanes $C_{15/17/19}$, with the highest concentration in the early Holocene (10.9–5.8 cal. ka BP) and late Holocene (since ~2.7 cal. ka BP) (Figure 7). The amount of long-chain alkanes *n*-$C_{27/29/31}$ continuously increases with time, while the middle-chain alkanes *n*-$C_{21/23/25}$ show a more differentiated pattern with low values of 0.1–2.9 µg/g covering the study period (Supp. Figure 1, available online). According to the *n*-alkane distribution, the sediment core could be separated into

Figure 6. (a) The principal component analysis (PCA) of lacustrine sediments from Zigetang Co and the resulting three clusters and (b) distribution patterns of n-alkanes in lake sediments within the individual clusters.
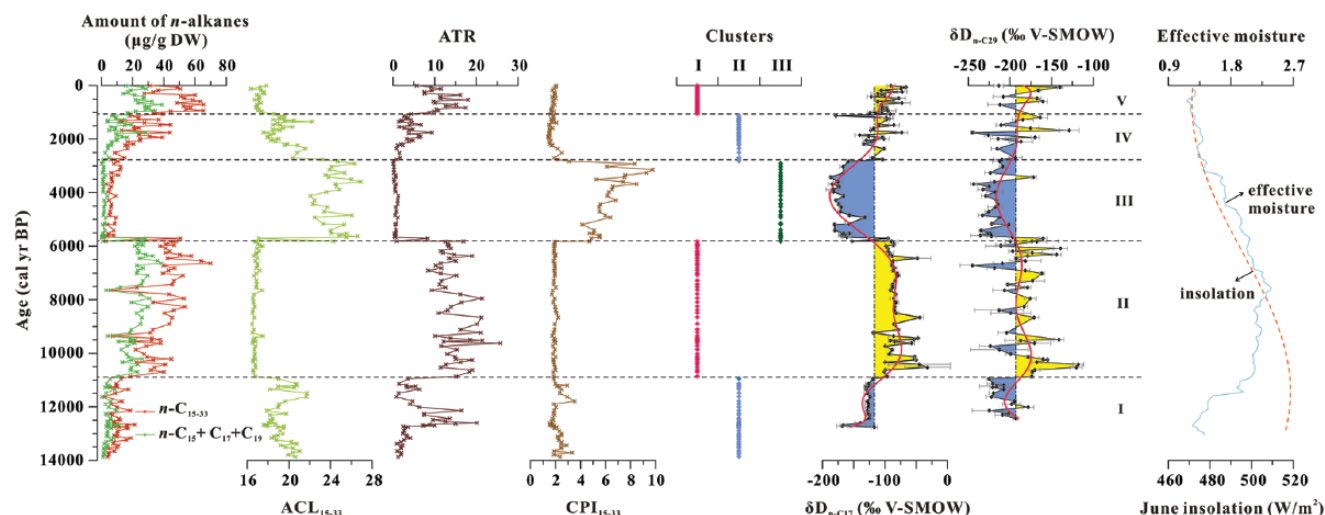
Figure 7. Total amounts of n-alkanes ($C_{15} + C_{17} + C_{19}$ and $C_{15–33}$), n-alkane indicator ratios (ACL, ATR, and CPI values), variations in distribution of Clusters I–III, and hydrogen isotope values (δD) of n-C_{17} and n-C_{29} of Zigetang Co record. The curve of effective moisture in monsoonal Central Asia (Herzschuh, 2006) and the solar insolation at 32°N in June (Berger and Loutre, 1991) are shown as well. The red solid lines represent the polynomial fit through the original data of δD values. Error bars illustrate the standard deviation of δD values.

three clusters using PCA (Figure 6). Sediments within clusters I and II are mainly controlled by short-chain n-alkanes such as C_{15}, C_{16}, and/or C_{17}. Samples combined in cluster II display higher relative abundances of long-chain odd-carbon-numbered n-alkanes ($\geq C_{21}$) than those in cluster I. The dominance in cluster III is shifted toward long-chain n-alkanes such as C_{29} and C_{31}.

The investigated sediment core can be roughly divided into five depositional periods according to variations in the amount of n-alkanes, ACL, and ATR (Figure 7). Period I (13.8–10.9 cal. ka BP) demonstrates that the amount of short-chain n-alkanes is relatively low with an average value of 4.4 μg/g dry weight. ATR values are slightly increased, whereas ACL values show an overall declining trend. The following Period II (10.9–5.8 cal. ka BP) reveals that the amount of short-chain n-alkanes is significantly increased except for abrupt decreases at approximately 9.3 and 7.6 cal. ka BP. ATR values are relatively high

with frequent fluctuations, while ACL values are low and stable with an average value of 16.8. During Period III (5.8–2.7 cal. ka BP), the amount of short-chain n-alkanes and ATR values reach their minimum with an average value of 1.48 μg/g dry weight and 0.6, respectively. In contrast, ACL values are higher than those in Period II. Period IV (2.7–1.1 cal. ka BP) is characterized by an obvious increase in the amount of short-chain n-alkanes and ATR values compared with the decreasing trends of ACL values. Period V (since ~1.1 cal. ka BP) displays the further increase in the amount of short-chain n-alkanes associated with much higher ATR values. Nevertheless, ACL values continuously do decline during this period. Clusters I and II, representing the microbial signals, dominate the composition of lake sediments during Periods I, II, IV, and V, while Cluster III as terrestrial indicator is only prevailing the record in Period III (5.8–2.7 cal. ka BP) (Figure 7).

Hydrogen isotope values of n-alkanes in lake sediments

In this study, we focus on the δD of n-C_{17} and n-C_{29} alkanes as aquatic and terrestrial biomarkers, which reflect the isotopic signal of the lake and inflow water, respectively (Günther et al., 2013; Pagani et al., 2006). Because of the low concentrations of n-alkanes, continuous and interpretable δD values are not available between 13.8 and 12.6 cal. ka BP. The value of δD$_{n\text{-}C17}$ and δD$_{n\text{-}C29}$ varied from −186.9‰ to −31.8‰ and from −244.9‰ to −118.1‰, respectively. Lower δD values are detected for n-C_{17} (−131 ± 13‰) and n-C_{29} (−209 ± 14‰) during the period from 12.6 to 10.9 cal. ka BP (Figure 7). And then, much greater δD values of n-C_{17} (−81 ± 18‰) occurred from 10.9 to 5.8 cal. ka BP, whereas δD values of n-C_{29} (−182 ± 26‰) fluctuated with high amplitudes. After that, δD values of n-C_{17} (−168 ± 12‰) and n-C_{29} (−217 ± 20‰) become more negative between 5.8 and 2.7 cal. ka BP. In the past 2.7 cal. ka BP, δD values of n-C_{17} (−112 ± 21‰) and n-C_{29} (−201 ± 29‰) show more positive trends.

Discussion

Provenance of sedimentary n-alkanes

Organic matter in lake sediments has different sources that contain complex environmental signals. Generally, the amount of sedimentary n-alkanes represents an excellent signal to discriminate the relative contribution between autochthonous and allochthonous organic matter (Eglinton and Hamilton, 1967; Ficken et al., 2000). Moreover, n-alkane proxies such as CPI and ACL values can also be applied to describe the organic matter in lacustrine sediments. Higher CPI and ACL values indicate relatively high contributions from the terrestrial vascular plants, whereas lower CPI and ACL values imply more aquatic and microbial influences and/or the decomposition effects of microorganism activities (Pu et al., 2010). For this study, the dominant n-alkanes are the short-chain homologues n-C_{15}, n-C_{16}, and/or n-C_{17} that cover almost the entire sediment core, resulting in low ACL and CPI values of 19.3 and 2.0, respectively. This illustrates that the sediments mainly consist of autochthonous organic matter such as aquatic algae, plankton, and photosynthetic bacteria. The microbial organism characteristics deduced from the n-alkane distributions are consistent with other geochemical records from the core ($^{13}C_{org}$, TOC/TN, and δ^{15}N values; Wu et al., 2007). As inferred from low concentrations of middle-chain n-alkanes $C_{23/25}$, aquatic macrophytes only played a minor role in the contribution to lake organic matter or were totally absent. The reduced growth of aquatic macrophytes can be attributed to the anoxic, hyper-saline, and alkaline settings in the lake water. This interpretation is supported by in situ investigations in this lake in 1999, 2002, 2006, and 2012, respectively (Li and Li, 2004; Supplementary Figure 2, available online). The long-chain alkanes n-C_{29} and/or n-C_{31} derived from allochthonous organic matter inputs (e.g. terrestrial plants) only control the n-alkane composition within short periods (5.8–2.7 cal. ka BP). This might be attributed to the microbial-dominated system and sparse vegetation cover under semi-dry and dry climate conditions in the Zigetang Co catchment.

Clearly, the meromictic endorheic saline lake system could be responsible for the high concentrated short-chain n-alkanes that derived from microbial organisms in Zigetang Co. Li et al. (2001b) propose a rapid salinity increase and an abrupt decrease in dissolved oxygen in the lake water with depth, as well as anoxic conditions at the bottom. Such a lake environment does not support significant phytoplankton or macrophyte productivity, but displays favorable conditions for benthic microorganism and/or bacteria proliferation. Photosynthetic organisms and complex microbial communities are responsible for a substantial fraction of primary production in other similar lake systems. These include cohesive benthic microbial mats in salt lakes in Australia (Bauld, 1986), bacterial and ciliate communities in the central Indian saline lakes (Sarkar et al., 2014), and extensive distribution of cyanobacterial mats in the saline ponds on the Christmas Island (Sachse and Sachs, 2008). In addition, the absence of phytoplankton organic matter in Zigetang Co might be attributed to the small and shallow lake basin. Regarding the uncertainty of this unusual n-alkanes distribution, further identification of n-alkanes sources should be performed with very specific proxies such as DNA.

Environmental significance of n-alkanes and their hydrogen isotopic composition

The growth of aquatic algae and the proliferation of bacteria are mainly controlled by temperature and salinity, so the amount of n-alkanes does not only indicate the bioproductivity but also reflects the climatic conditions. Additionally, n-alkane indicator ratios enable semi-quantitative interpretation of organic matter sources and climate evolution in geological periods. The ATR, for instance, has been increasingly used to discriminate the organic origin, which can be a signal of climate conditions (Herzschuh et al., 2005). Higher ATR values correspond to relatively warm periods, and lower values reflect cool periods. Moreover, the compound-specific hydrogen isotope ratios (δD) of n-alkanes reflect the source water and, therefore, changes in the hydrological cycles as well as in the climate (Mügler et al., 2010; Wang et al., 2013). The δD values of terrestrial n-alkanes (e.g. C_{29}) reflect the meteoric water modified by evapotranspiration and/or other meteorological factors, whereas the δD values of aquatic n-alkanes (e.g. C_{17}) record the isotopic composition of the corresponding lake water modified by evaporation (Günther et al., 2013; Pagani et al., 2006). In addition, aquatic n-alkane δD values can be strongly influenced by salinity. An increase in salinity resulting from an excess of evaporation over precipitation is usually accompanied by an increase in water δD values and vice versa (Sachse and Sachs, 2008).

Stage I (8.8–6.9 m, 13.8–10.9 cal. ka BP). As inferred from the low ATR values, the oldest period is characterized by a cold environment. Clearly, the cold conditions are not conducive to the growth of algae and plankton and, hence, resulted in the relative low amounts of short-chain n-alkanes. The lower δD values of n-C_{17} and n-C_{29} indicate a weak evaporation of the lake water as well as a weak evapotranspiration in the catchment. As a consequence, more effective moisture was available in the lake catchment.

Stage II (6.9–3.9 m, 10.9–5.8 cal. ka BP). The highest amount of short-chain n-alkanes is closely linked with substantial anaerobic microbial decomposition of organic matter because of a rise in insolation-driven temperature (Figure 7). Consequently, strongly decreased ACL values and increased ATR values are recorded during this period. Sharp decreases in the amount of n-alkanes are observed at approximately 9.3 and 7.6 cal. ka BP, which are in accordance with pollen and ostracod records (Herzschuh et al., 2006; Zhang et al., 2014). Likewise, the occurrence of severe climate fluctuations during the early Holocene has also been displayed in other Tibetan lake records (e.g. Gasse et al., 1996; Shen et al., 2005). The trigger for these fluctuations, however, has not yet been traced. The increasing δD values of n-C_{17} point to a reduced lake volume caused by higher temperature–induced evaporation in the catchment. The δD values of n-C_{29} are higher but display great fluctuations pointing to rather unstable climate conditions. As inferred from the pollen record in Zigetang Co catchment, the early Holocene is furthermore characterized by a general drier trend with strong vegetation and climate instability (Herzschuh et al., 2006). Solar forcing has a rather direct

influence on Tibetan temperature and is likely responsible for the drier early Holocene. In general, the insolation-driven intensification of the monsoon led to higher precipitation amounts and also higher temperatures at the beginning of the Holocene. The enhanced evaporation at Zigetang Co could possibly have outweighed the increase in precipitation and, therefore, result in significant lower effective moisture availability and enriched hydrogen isotopes values in the lake. The lack of glacial meltwater input in Zigetang Co would provide isotopically depleted water and, would finally, enforce the trend to greater δD values in the lake water. Enhanced local recycling of air masses could also cause an isotopic enrichment and cannot be excluded.

Stage III (3.9–2.0 m, 5.8–2.7 cal. ka BP). The amount of *n*-alkanes decreases abruptly, suggesting low microorganism activities at that time. As inferred from the highest CPI values and the lowest values of ATR, enhanced terrestrial inputs to the lake are recorded probably because of the increasing moisture availability. This is in accordance with the dominance of *Cyperaceae* in this region around 5000 cal. yr BP (Herzschuh et al., 2006). Simultaneous low δD values of *n*-C_{17} and *n*-C_{29} point to a higher lake volume and more plant available water, which is attributed either to lower evaporation associated with the weakening solar insolation or higher precipitation (Figure 7). In agreement with our record, carbonate and soluble salt records from Zigetang Co also suggest the occurrence of humid conditions connected with the desalination of the lake and the rise of the lake volume during the periods of 5.0–4.7 cal. ka BP, 4.0–3.8 cal. ka BP, and 3.1–2.7 cal. ka BP, respectively (Li et al., 2009; Supplementary Figure 3, available online). Likewise, Herzschuh et al. (2006) propose that the wetter climate conditions that occurred in Zigetang Co catchment are associated with the dominating temperature steppe vegetation from 7.3 to 4.4 cal. ka BP.

Stage IV (2.0–0.8 m, 2.7–1.1 cal. ka BP). The enhanced biomass production of lacustrine algae and bacteria connected to higher amounts of short-chain *n*-alkanes result in decreasing ACL and CPI values. Warmer conditions can be indicated by increasing trends for ATR values in this period. Rising temperatures could evoke higher evaporation of the lake water and resultant higher salinity that might reduce the exchange of water across the cell membranes. As a result, intracellular water will be recycled and become progressively D-enriched which will be subsequently reflected in the lipids (e.g. positive δD values of *n*-C_{17}). The δD values of *n*-C_{29} are highly variable but generally correspond to more arid conditions. This is probably attributed to the decreasing monsoonal precipitation because of the reduced solar irradiance.

Stage V (0.8–0 m, 1.1–0 cal. ka BP). The further increasing amount of short-chain *n*-alkanes indicates enhanced biological productivity associated with the 'Medieval Warm Period'. This change is accompanied by increasing ATR values and declining ACL values. There is a general trend toward drier climatic conditions with short occurrence of humid environment as inferred from the higher δD values of *n*-C_{29}, which is in line with ostracod shell isotope records (Zhang et al., 2014). This generally dry period is interrupted by short intervals of humid conditions that might be connected to transient wet phases.

Possible forcing mechanism for Holocene effective moisture evolution

Effective moisture availability is essential for the evaluation on atmospheric water vapor as well as vegetation composition and distribution in the region, which is primarily affected by precipitation, temperature, evaporation, lake morphology, and other climatic as well as hydrological driving factors (Maslin and Burns,

2000). There is no glacier distribution in the catchment, and the precipitation controlled by the Indian summer monsoon is the main water supply for Zigetang Co. Therefore, the expansion and contraction of the lake volume directly reflect changes of moisture availability dominated by monsoon-derived precipitation and temperature-induced evaporation. As discussed above, δD values of *n*-C_{17} from Zigetang Co enable us to investigate the evaporation-induced lake-level changes. Consequently, our results can be compared with neighboring lake records from Paru Co (Bird et al., 2014), Nam Co (Günther et al., 2015; Mügler et al., 2010), and Siling Co (Gu et al., 1993) to better understand Holocene effective moisture evolution and potential drivers in the Zigetang Co catchment (Figures 1 and 8).

During the period of 10.9–5.8 cal. ka BP (early to mid-Holocene), as inferred from the δD values of *n*-C_{17}, the lower lake level and reduced effective moisture availability are recorded at Zigetang Co. In contrast, Herzschuh (2006) pointed out that the strong summer monsoon and humid conditions are typical for the early Holocene in monsoonal domains on the Tibetan Plateau. In case of Paru Co, minimum δD$_{wax}$ values are observed, suggesting much effective moisture in this period linked to enhanced rainfall from rapid strengthening of Indian summer monsoon (Bird et al., 2014). Likewise, the Nam Co record indicated by the decreasing δD values reveals an episode of predominantly humid climate and high lake level during the early Holocene (Günther et al., 2015). In addition, wet conditions displayed by lower δ18O values associated with intensified monsoon circulation remained until around 6.2–6.0 cal. ka BP at Siling Co (Gu et al., 1993). Given the same climate zone for these lakes because of the close location (Figure 1), we assume that they are influenced by similar temperature and/or precipitation intensity. The significant discrepancy among these lake systems would be caused by differences in water supplies to the lakes such as the glacial meltwater contributions and variable evaporation intensities. Nam Co and Paru Co (~300 and ~500 km southeast of Zigetang Co, respectively) are located in the Nyainqentanglha Mountains that are covered by extensive glaciers impacting the lake water budget surrounding the region. Siling Co (~200 km southwest of Zigetang Co) is also strongly affected by the glacial melt supplies from Tanggula Mountains. In comparison, the water supply at Zigetang Co only depends on precipitation and seasonal inflows due to lacking glacial meltwater inputs. The climate warming during the early Holocene on the Tibetan Plateau is induced by strong solar insolation in the Northern Hemisphere (Kutzbach, 1981). Higher temperature would result in an enhanced evaporation and higher δD values. However, warmer conditions also accelerate the melting of ice and snow, providing a further moisture source and leading to an increasing humidity in many lake systems (Chen et al., 2008). The input of glacial meltwater in Nam Co, Paru Co, and Siling Co, for instance, counteract the evaporation of the lake water and is finally needed to establish humid conditions and high lake volumes in these lake systems displayed by lower δD values. In contrast, Zigetang Co is characterized by less effective moisture availability and much greater δD values during the period. This may be attributed to the missing glacial meltwater input in the lake. Consequently, the temperature-induced evaporation could outweigh the increased monsoonal precipitation and, finally, result in a decreasing lake volume and more enriched δD values in Zigetang Co.

Our inference of the onset of higher effective moisture phases at about 5.8 cal. ka BP contrasts with palaeoclimate records from neighboring lakes since the wettest conditions are usually not recorded that late after the insolation maximum. The moisture availability in the Zigetang Co catchment is more influenced by temperature-induced evaporation than by precipitation because of its marginal position within the Indian summer monsoon. As a consequence, the decreasing summer insolation over the later half
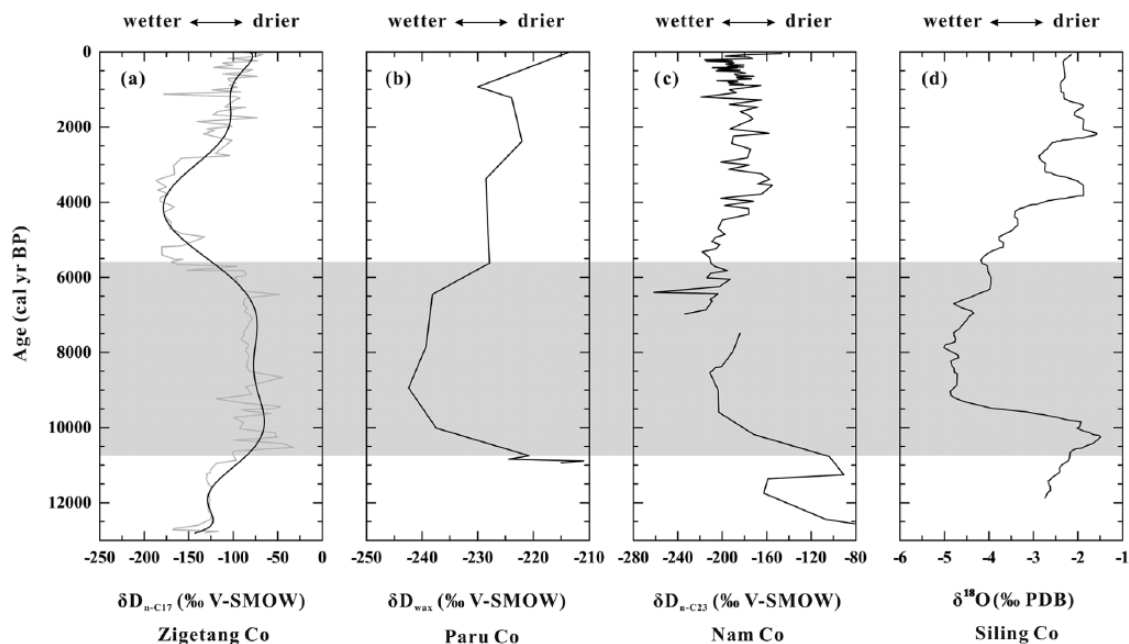
Figure 8. Comparison of the Holocene moisture evolution in different Tibetan lake systems. (a) $\delta D_{n\text{-}C17}$ values from Zigetang Co (this study; raw data as thin gray line, and 10-point smoothed data in bold black line), (b) δD_{wax} values from Paru Co (Bird et al., 2014), (c) $\delta D_{n\text{-}C23}$ values from Nam Co (Günther et al., 2015; Mügler et al., 2010), and (d) $\delta^{18}O$ values from Siling Co (Gu et al., 1993). The gray box represents the drier conditions at Zigetang Co in contrast with other neighboring lake records.

of the Holocene (Figure 7) caused the reduced evaporation and ultimately led to higher effective moisture availability in the region. As the transition region of the monsoon and Westerlies on the Tibetan Plateau, humid conditions at Zigetang Co catchment during the middle Holocene were created to a minor extent by the Westerlies with the weakening of the Indian monsoon linked to the reduction of summer solar radiation in the Northern Hemisphere. In addition, more water vapors would be transported by continental air mass circulation from inland lakes and rivers and, therefore, would establish relative humid environments in the catchment.

The major shift from wetter to drier conditions at Zigetang Co around 2.7 cal. ka BP is in good agreement with other records in monsoonal domains (e.g. Gu et al., 1993; Mügler et al., 2010; Wu et al., 2006). Nevertheless, the exact time of dry condition appearance differs between the individual sites because of inconsistent geological and hydrological settings as well as uncertain age models. Siling Co and Nam Co sediments show episodes of much greater dryness around 2.4–1.4 and ~1.5 cal. ka BP, respectively (Gu et al., 1993; Mügler et al., 2010). The sedimentary record from Lake Cuoe also suggests arid climate conditions since ~3.0 cal. ka BP (Wu et al., 2006). These dry conditions are probably attributed to the decreasing monsoonal precipitation that is mainly driven by external forcing and solar variability in the Northern Hemisphere.

Conclusion

Our results highlight contrasting observations of drier and wetter conditions from different lake catchments during the early Holocene on the Tibetan Plateau. The complex relationship of summer radiation–induced temperature, evaporation, and precipitation increases is mainly responsible for the observed spatial heterogeneities in effective moisture availability. Increasing temperature and precipitation might result in more effective moisture in many sites, but, in comparison, might lead to less moisture availability if the temperature-driven evaporation exceeds the increase in the precipitation, especially if the buffering capacities of glaciers are missing in the catchment. The pronounced differences in local

environments such as topography, vegetation cover, discharge, and moisture recycling additionally contribute to the asynchronous climate history in the region. Consequently, more records with reliable proxies and chronologies in the region are needed to trace the effects of regional heterogeneity on the reconstruction of the Holocene monsoon dynamics on the Tibetan Plateau.

References

Aichner B, Herzschuh U, Wilkes H et al. (2010) δD values of *n*-alkanes in Tibetan lake sediments and aquatic macrophytes – A surface sediment study and application to a 16 ka record from Lake Koucha. *Organic Geochemistry* 41: 779–790.

Bauld J (1986) Benthic microbial communities of Australian saline lakes. *Limnology in Australia* 61: 96–111.

Berger A and Loutre MF (1991) Insolation values for the climate of the last 10 million years. *Quaternary Science Reviews* 10: 297–317.

Bird BW, Polisar PJ, Lei YB et al. (2014) A Tibetan lake sediment record of Holocene Indian summer monsoon variability. *Earth and Planetary Science Letters* 399: 92–102.

Blaauw M (2010) Methods and code for 'classical' age-modelling of radiocarbon sequences. *Quaternary Geochronology* 5: 512–518.

Blaauw M and Christen JA (2005) Radiocarbon peat chronologies and environmental change. *Journal of the Royal Statistical Society Series C: Applied Statistics* 54: 805–816.

Blyth A, Baker A, Thomas LE et al. (2011) A 2000-year lipid biomarker record preserved in a stalagmite from north-west Scotland. *Journal of Quaternary Science* 26: 326–334.

Bouloubassi I, Saliot A, Rougerie F et al. (1992) Hydrocarbon geochemistry in coral reef waters, French Polynesia. In: Kharaka YK and Maest AS (eds) *Water-Rock Interaction*, vol. 1. Rotterdam: Balkema, pp. 271–274.

Bray EE and Evans ED (1961) Distribution of *n*-paraffins as a clue to recognition of source beds. *Geochimica et Cosmochimica Acta* 22: 2–15.

Chen FH, Yu ZC, Yang ML et al. (2008) Holocene moisture evolution in arid central Asian and its out-of-phase relationship with Asian monsoon history. *Quaternary Science Reviews* 27: 351–364.

Cranwell PA, Eglinton G and Robinson N (1987) Lipids of aquatic organisms as potential contributors to lacustrine sediments–II. *Organic Geochemistry* 11: 513–527.

Eglinton G and Hamilton RJ (1967) Leaf epicuticular waxes. *Science* 156: 1322–1335.

Ficken KJ, Li B, Swain DL et al. (2000) An *n*-alkane proxy for sedimentary input of submerged/floating freshwater aquatic macrophytes. *Organic Geochemistry* 31: 745–749.

Gasse F, Fontes JC, Campo EV et al. (1996) Holocene environmental changes in Bangong Co basin (Western Tibet). Part 4: Discussion and conclusions. *Palaeogeography, Palaeoclimatology, Palaeoecology* 120: 79–92.

Gu ZY, Liu JQ, Yuan BY et al. (1993) Monsoon variations of the Qinghai-Xizang Plateau during the last 12,000 years – Geochemical evidence from the sediments in the Siling Lake. *Chinese Science Bulletin* 38: 577–581.

Guan ZH, Chen CY, Qu YX et al. (1984) *The Rivers and Lakes in Tibet*. Beijing: Science Press, pp. 159–168 (in Chinese).

Günther F, Mügler L, Aichner B et al. (2013) A synthesis of hydrogen isotope variability and its hydrological significance at the Qinghai–Tibetan Plateau. *Quaternary International* 313: 3–16.

Günther F, Mügler L, Mäusbacher R et al. (2011) Response of δD values of sedimentary *n*-alkanes to variations in source water isotope signals and climate proxies at lake Nam Co, Tibetan Plateau. *Quaternary International* 236: 82–90.

Günther F, Witt R, Schouten S et al. (2015) Quaternary ecological responses and impacts of the Indian Ocean Summer Monsoon at Nam Co, Southern Tibetan Plateau. *Quaternary Science Reviews* 112: 66–77.

Han J and Calvin M (1969) Hydrocarbon distribution of algae and bacteria, and microbiological activity in sediments. *Proceeding of the National Academy of Sciences of the United States of America* 64: 436–443.

Herzschuh U (2006) Palaeo-moisture evolution at the margins of the Asian monsoon during the last 50 ka. *Quaternary Science Review* 25: 163–178.

Herzschuh U, Winter K, Wünnemann B et al. (2006) A general cooling trend on the central Tibetan Plateau throughout the Holocene recorded by the Lake Zigetang pollen spectra. *Quaternary International* 154: 113–121.

Herzschuh U, Zhang CJ, Mischke S et al. (2005) A late Quaternary lake record from the Qilian Mountains (NW China): Evolution of the primary production and the water depth reconstructed from macrofossil, pollen, biomarker, and isotope data. *Global and Planetary Change* 46: 361–379.

Hou JZ, D'Andrea WJ and Liu ZH (2012) The influence of ¹⁴C reservoir age on interpretation of paleolimnological records from the Tibetan Plateau. *Quaternary Science Reviews* 48: 67–79.

Hu CY, Henderson GM, Huang JH et al. (2008) Quantification of Holocene Asian monsoon rainfall from spatially separated cave records. *Earth and Planetary Science Letters* 266: 221–232.

Huang Y, Shuman B, Wang Y et al. (2004) Hydrogen isotope ratios of individual lipids in lake sediments as novel tracers of climatic and environmental change: A surface sediment test. *Journal of Paleolimnology* 31: 363–375.

Jeng WL (2006) Higher plant *n*-alkane average chain length as an indicator of petrogenic hydrocarbon contamination in marine sediments. *Marine Chemistry* 102: 242–251.

Kutzbach JE (1981) Monsoon climate of the early Holocene: Climate experiment using the earth's orbital parameters for 9000 years ago. *Science* 214: 59–61.

Kutzbach JE, Prell WL and Ruddiman WF (1993) Sensitivity of Eurasian climate to surface uplift of the Tibetan Plateau. *Journal of Geology* 101: 177–190.

Li SJ and Li WC (2004) Hydrochemistry in meromictic Lake Zige Tangco, Central Tibetan Plateau. *Asian Journal of Water, Environment and Pollution* 1: 1–4.

Li SJ, Wünnemann B, Xia WL et al. (2009) A preliminary study of the Holocene lake level changes and their causes derived from the sediment record of Zigetang Lake, Tibetan Plateau. *Earth Science Frontiers* 16: 162–167 (in Chinese).

Li WC, Li SJ and Pu PM (2001a) Estimates of plateau lake evaporation: A case study of Zige Tangco. *Journal of Lake Sciences* 13: 227–232.(in Chinese).

Li WC, Li SJ, Yin Y et al. (2001b) The discovery of semi-mixed lakes and its significance on Tibetan Plateau. *Science in China Series D: Earth Sciences* 30: 269–272 (in Chinese).

Liu WG and Huang YS (2005) Compound specific D/H ratios and molecular distribution of higher plant leaf waxes as novel paleoenvironmental indicators in the Chinese Loess Plateau. *Organic Geochemistry* 36: 15–23.

Liu XD, Kutzbach JE, Liu ZY et al. (2003) The Tibetan Plateau as amplifier of orbital-scale variability of the East Asian monsoon. *Geophysical Research Letters* 30: 1–4.

Maslin MA and Burns SJ (2000) Reconstruction of the Amazon basin effective moisture availability over the past 14,000 years. *Science* 290: 2285–2287.

Meyers PA (1997) Organic geochemical proxies of paleoceanographic, paleolimnologic, and paleoclimatic processes. *Organic Geochemistry* 27: 213–250.

Meyers PA (2003) Application of organic geochemistry to paleolimnological reconstructions: A summary of examples from the Laurentian Great Lakes. *Organic Geochemistry* 34: 261–289.

Miehe G, Miehe S, Schlutz F et al. (2006) Palaeoecological and experimental evidence of former forest and woodlands in the treeless desert pastures of Southern Tibet (Lhasa, A.R. Xizang, China). *Palaeogeography, Palaeoclimatology, Palaeoecology* 242: 54–67.

Mügler I, Gleixner G, Günther F et al. (2010) A multi-proxy approach to reconstruct hydrological changes and Holocene climate development of Nam Co, Central Tibet. *Journal of Paleolimnology* 43: 625–648.

Pagani M, Pedentchouk N, Huber M et al. (2006) Arctic hydrology during global warming at the Palaeocene/Eocene thermal maximum. *Nature* 442: 671–675.

Peleiero C (2003) Terrigenous n-alkane input in the South China Sea: High-resolution records and surface sediments. *Chemical Geology* 200: 89–103.

Poynter J and Eglinton G (1990) Molecular composition of three sediments from hole 717C: The Bengal fan. *Proceedings of the Ocean Drilling Program, Scientific Results* 116: 155–161.

Pu Y, Zhang HC, Lei GL et al. (2010) Climate variability record by *n*-alkanes of paleolake sediment in Qaidam Basin on the

northeast Tibetan in late MIS3. *Science in China Series D: Earth Sciences* 53: 863–870.

Rieley G, Collier RJ, Jones DM et al. (1991) The biogeochemistry of Ellesmere Lake, U.K. – I: Source correlation of leaf wax inputs to the sedimentary lipid record. *Organic Geochemistry* 17: 901–912.

Sachse D and Sachs JP (2008) Inverse relationship between D/H fractionation in cyanobacterial lipids and salinity in Christmas Island saline ponds. *Geochimica et Cosmochimica Acta* 72: 793–806.

Sachse D, Billault I, Bowen GJ et al. (2012) Molecular paleohydrology: Interpreting the hydrogen-isotopic composition of lipid biomarkers from photosynthesizing organisms. *Earth and Planetary Science Letters* 40: 221–249.

Sarkar S, Wilkes H, Prasad S et al. (2014) Spatial heterogeneity in lipid biomarker distributions in the catchment and sediments of a crater lake in central India. *Organic Geochemistry* 66: 125–136.

Schefuss E, Schouten S and Schneider RR (2005) Climatic controls on central African hydrology during the past 20,000 years. *Nature* 437: 1003–1006.

Seki O, Mayer PA, Kawamura K et al. (2009) Hydrogen isotopic ratios of plant wax *n*-alkanes in a peat bog deposited in northeast China during the last 16 kyr. *Organic Geochemistry* 40: 671–677.

Shen J, Liu XQ, Wang SM et al. (2005) Palaeoclimatic changes in the Qinghai Lake area during the last 18,000 years. *Quaternary International* 139: 131–140.

Thompson LG, Yao TD, Mosley-Thompson E et al. (2000) A high-resolution millennial record of the south Asian monsoon from Himalayan ice cores. *Science* 289: 1916–1919.

Wang SM and Dou HS (1998) *Lake in China*. Beijing: Science Press, pp. 408–409 (in Chinese).

Wang Z, Liu WG, Liu ZH et al. (2013) A 1700-year *n*-alkanes hydrogen isotope record of moisture changes in sediments from Lake Sugan in the Qaidam Basin, northeastern Tibetan Plateau. *The Holocene*. Epub ahead of print 15 May. DOI: 10.1177/0959683613486941.

Wu YH, Lücke A, Jin ZD et al. (2006) Holocene climate development on the central Tibetan Plateau: A sedimentary record from Cuoe Lake. *Palaeogeography, Palaeoclimatology, Palaeoecology* 234: 328–340.

Wu YH, Lücke A, Wünnemann B et al. (2007) Holocene climate change in the Central Tibetan Plateau inferred by lacustrine sediment geochemical records. *Science in China Series D: Earth Sciences* 50: 1548–1555.

Xie SC, Chen FH, Wang ZY et al. (2003) Lipid distribution in loess-paleosol sequence from northwest China. *Organic Geochemistry* 34: 1071–1079.

Xie SC, Yao TD, Kang SC et al. (2000) Geochemical analyses of a Himalayan snowpit profile: Implication for atmospheric pollution and climate. *Organic Geochemistry* 31: 15–23.

Yao TD and Zhu LP (2006) The response of environmental changes on Tibetan Plateau to global changes and adaptation strategy. *Advances in Earth Science* 21: 459–464 (in Chinese).

Zhang HL, Liu QL, Li SJ et al. (2014) Holocene environmental changes derived from ostracode shell stable isotope in sediment core of Zigetang Lake, Tibetan Plateau. *Mountain Research* 32: 373–379 (in Chinese).

Zhao Y, Yu ZC and Zhao WW (2011) Holocene vegetation and climate histories in the eastern Tibetan Plateau: Controls by insolation-driven temperature or monsoon-derived precipitation changes? *Quaternary Science Reviews* 30: 1173–1184.

Zheng YH, Zhou WJ, Mayer PA et al. (2007) Lipid biomarkers in the Zoige-Hongyuan peat deposit: Indicator of Holocene climate changes in West China. *Organic Geochemistry* 38: 1927–1940.

Zhou WJ, Yu XF, Timothy Jull AJ et al. (2004) High-resolution evidence from southern China of an early Holocene optimum and a mid-Holocene dry event during the past 18,000 years. *Quaternary Research* 62: 39–48.

Zhu LP, Wu YH, Wang JB et al. (2008) Environmental changes since 8.4 ka reflected in the lacustrine core sediments from Nam Co, central Tibetan Plateau, China. *The Holocene* 18: 831–839.